# Nitrogenase Reduction of Carbon Disulfide: Freeze-Quench EPR and ENDOR Evidence for Three Sequential Intermediates with Cluster-Bound Carbon Moieties†

Matthew J. Ryle,‡ Hong-In Lee,§ Lance C. Seefeldt,*,‡ and Brian M. Hoffman*,§

*Department of Chemistry and Biochemistry, Utah State University, Logan, Utah 84322, and Department of Chemistry, Northwestern University, Evanston, Illinois 60208*

*Received August 16, 1999; Revised Manuscript Received October 21, 1999*

ABSTRACT: Freeze-quenching of nitrogenase during reduction of carbon disulfide ($CS_2$) was previously shown to result in the appearance of a novel EPR signal ($g = 2.21$, 1.99, and 1.97) not previously associated with any of the oxidation states of the nitrogenase metal clusters. In the present work, freeze-quench X- and Q-band EPR and Q-band $^{13}C$ electron nuclear double resonance (ENDOR) spectroscopic studies of nitrogenase during $CS_2$ reduction disclose the sequential formation of three distinct intermediates with a carbon-containing fragment of $CS_2$ bound to a metal cluster inferred to be the molybdenum−iron cofactor. Modeling of the Q-band (35 GHz) EPR spectrum of freeze-trapped samples of nitrogenase during turnover with $CS_2$ allowed assignment of three signals designated "a" ($g = 2.035$, 1.982, 1.973), "b" ($g = 2.111$, 2.002, and 1.956), and "c" ($g = 2.211$, 1.996, and 1.978). Freezing samples at varying times after initiation of the reaction reveals that signals "a", "b", and "c" appear and disappear in sequential order. Signal "a" reaches a maximal intensity at 25 s; signal "b" achieves maximal intensity at 60 s; and signal "c" shows maximal intensity at 100 s. To characterize the intermediates, $^{13}CS_2$ was used as a substrate, and freeze-trapped turnover samples were examined by Q-band $^{13}C$ ENDOR spectroscopy. Each EPR signal ("a", "b", and "c") gave rise to a distinct $^{13}C$ signal, with hyperfine coupling constants of 4.9 MHz for $^{13}C_a$, 1.8 MHz for $^{13}C_b$, and 2.7 MHz for $^{13}C_c$. Models for the sequential formation of intermediates during nitrogenase reduction of $CS_2$ are discussed.

The metalloenzyme nitrogenase is responsible for biological reduction of $N_2$ to ammonia (*1*). In addition, nitrogenase reduces protons to form $H_2$ as part of the reaction mechanism, with $H_2$ formation accounting for 25−100% of the flow of electrons through the enzyme (*2*−*4*). The hydrolysis of at least 2 ATP molecules to 2 ADP and 2 $P_i$ is coupled to the transfer of each electron through the enzyme (*5*). Nitrogenase is a complex metalloprotein composed of two proteins called the iron (Fe) protein and the molybdenum−iron (MoFe)[1] protein. The MoFe protein, an $\alpha_2\beta_2$ tetramer, contains two biologically unique metal clusters (one each per $\alpha\beta$ subdomain) called the FeMo cofactor ([1Mo-7Fe-8S-1homocitrate]) and the P-cluster ([8Fe-7S]) (*6*). FeMo cofactor is the site of substrate binding and reduction (*7*), while each P-cluster appears to serve as an electron-transfer intermediate between the Fe protein and FeMo cofactor (*8*−*12*). The Fe protein serves as a specific electron-transfer protein to the MoFe protein, and contains two ATP binding and hydrolysis sites (*13*).

Despite the availability of the X-ray structures of both nitrogenase components (*6*, *13*) and the keen interest in achieving a molecular understanding of $N_2$ binding and reduction by nitrogenase, relatively little direct experimental evidence on this process is available because nitrogenase does not bind $N_2$ or any other known substrate in the resting state, but rather only under enzymatic turnover. The three approaches that have been used, individually or in combination, to address substrate binding and reduction are as follows: (1) quenching nitrogenase during turnover; (2) examining alternative substrates or inhibitors; and (3) constructing site-specifically modified proteins. For example, acid or base quenching of nitrogenase during reduction of $N_2$ revealed detectable levels of hydrazine, suggesting this as a reaction intermediate during $N_2$ reduction to $NH_3$ (*14*). Likewise, freeze-quenching of nitrogenase during reduction of protons (*11*, *15*, *16*), acetylene (*16*), or $N_2$ (*17*) or in the presence of CO as an inhibitor (*15*, *17*) has revealed new EPR signals, suggesting trapping of intermediates. However, only recently have $^{13}C$ ENDOR studies of $^{13}CO$-inhibited forms provided the first direct information about the binding of a diatom, in this case the inhibitor CO, to the nitrogenase MoFe protein (*18*−*20*). More recently, freeze-quenching of nitrogenase with an amino acid substitution near the FeMo cofactor during reduction of the substrate acetylene has revealed an EPR active species that likely represents a trapped intermediate (Hales, personal communication).

† This work was supported by National Science Foundation Grants MCB-9722937 to L.C.S. and MCB-9904018 to B.M.H. and by USDA Grant 97-37305-4879 to B.M.H.

* Address correspondence to L.C.S. at the Department of Chemistry and Biochemistry, Utah State University, Logan, UT 84322-0300; Phone: (435) 797-3964, Fax: (435) 797-3390, E-mail: seefeldt@cc.usu.edu. Address correspondence to B.M.H. at the Department of Chemistry, Northwestern University, Evanston, IL 60208-3113; Phone: (847) 491-7595, Fax: (847) 491-7713, E-mail: bmh@nwu.edu.

‡ Utah State University.

§ Northwestern University.

[1] Abbreviations: Fe protein, iron protein of nitrogenase; MoFe protein, molybdenum−iron protein of nitrogenase; *Av*1, MoFe protein from *Azotobacter vinelandii*; *Av2*, Fe protein from *Azotobacter vinelandii*; MOPS, 3-(*N*-morpholino)propanesulfonic acid; Tris, tris(hydroxymethyl)aminomethane; EPR, electron paramagnetic resonance spectroscopy; ENDOR, electron−nuclear double resonance spectroscopy; RF, radio frequency.

10.1021/bi9919100 CCC: $19.00 
Published on Web 01/12/2000

Nitrogenase reduces the alternative substrate carbon disulfide ($CS_2$) to $H_2S$ and an undefined CS compound, and recently we found that freeze-quenching of nitrogenase during this reaction resulted in a new EPR signal not previously reported, suggesting that an intermediate state had been trapped (*21*). In the present work, freeze-quench X- and Q-band EPR spectroscopies have disclosed the sequential formation of three distinct intermediates during reduction of $CS_2$ by nitrogenase, and $^{13}$C-ENDOR spectroscopy has shown that each contains a carbon-containing fragment of $^{13}CS_2$.

## EXPERIMENTAL PROCEDURES

*Expression and Purification of Nitrogenase Proteins. Azotobacter vinelandii* cells were grown as previously described (*22*). Nitrogenase Fe and MoFe proteins were purified to apparent homogeneity (*23, 24*) as judged by migration in SDS−PAGE with Coomassie blue staining (*25*). Protein concentrations were determined by a modified biuret method using bovine serum albumin as the standard (*26*). All manipulations of proteins were conducted in the absence of oxygen in sealed serum vials.

*Acetylene and Proton Reduction Activities.* Acetylene and proton reduction activity assays were conducted as previously described (*27*). Both the Fe protein and the MoFe protein were determined to have specific activities greater than 1900 nmol of acetylene reduced·min$^{-1}$·(mg of protein)$^{-1}$. Substrate reduction assays all contained a MgATP regenerating system (*24*). All assays were conducted at 30 °C with shaking. The reactions were initiated by the addition of Fe protein, and quenched by the addition of 250 $\mu$L of 2.5 M $H_2SO_4$.

*Preparation of $CS_2$ EPR and ENDOR Samples.* Samples for EPR analysis were prepared in 100 mM MOPS buffer, pH 7.0, that contained 30 mM MgATP, 70 mM phosphocreatine, 100 mM dithionite, and 3 mg/mL creatine phosphokinase. Unless otherwise noted, assay vials contained an initial $CS_2$ (J. T. Baker, Phillipsburg, NJ) concentration of 1 mM added from a 100 mM stock solution that was prepared by adding 6 $\mu$L of aerobic $CS_2$ to 1 mL of argon-purged dimethyl sulfoxide in a sealed serum vial fitted with a butyl stopper (*21*). To minimize the EPR signal due to the Fe protein, samples contained a 0.5 to 1 molar ratio of Fe protein to MoFe protein. All reaction components, except for the Fe protein, were placed in a sealed 6 mL serum vial under 101 kPa of argon. The reaction was initiated by the addition of the Fe protein, and then allowed to react inside the serum vial until 15 s prior to freezing when 250 $\mu$L of assay solution was transferred into a septum-sealed, argon-purged, 4 mm quartz EPR tube using a syringe. Samples were frozen in liquid nitrogen at the times indicated. The freezing time for each sample was estimated to be ~5 s.

Samples with $^{13}CS_2$ for ENDOR analysis were prepared in 100 mM MOPS buffer, pH 7.0, that contained 30 mM MgATP, 70 mM phosphocreatine, 100 mM dithionite, 3 mg/mL creatine phosphokinase, 250 $\mu$M MoFe protein, and an initial $^{13}CS_2$ (Cambridge Isotope Laboratories, Inc., Andover, MA) concentration of 1 mM. All reaction components, except for the Fe protein, were placed in a sealed 6 mL serum vial under 101 kPa of argon. The reaction was initiated by the addition of the Fe protein to a final concentration of 125 $\mu$M. The solution was mixed and allowed to react for 60 s prior to transferring 80 $\mu$L of assay solution into a septum-sealed, argon-purged, quartz ENDOR tube using a Hamilton syringe. The sample was immediately frozen in liquid nitrogen.

*X-Band EPR and Q-Band (35 GHz) EPR and ENDOR Spectroscopies.* X-band (9.64 GHz) EPR spectra were recorded on a Bruker ESP300E spectrometer equipped with a dual mode cavity and an Oxford ESR 900 liquid helium cryostat. All other parameters are noted in the figure legends.

Q-band CW EPR and ENDOR spectra were obtained at 2 K on a modified Varian E-110 spectrometer equipped with a helium immersion dewar (*28*). The spectra were recorded in dispersion mode using 100 kHz field modulation under "rapid passage" conditions, and spectra represent the absorption line shape, not its derivative (*29, 30*). For ENDOR, the bandwidth of radio frequency (RF) is broadened to 100 kHz to increase the signal-to-noise ratio (*31*). The first-order ENDOR spectrum of an $I = 1/2$ nucleus with $I = 1/2$ for a single orientation of a paramagnetic center consists of a doublet with frequencies given by eq 1 (*32*):

$$\nu_{\pm} = |\nu_N \pm A/2| \quad (1)$$

Here, $\nu_N$ is the nuclear Larmor frequency and $A$ is the orientation-dependent hyperfine coupling constant of the coupled nucleus. In the present study, $\nu_N < |A/2|$, and the observed doublets are centered at the Larmor frequency and separated by $A$. Spectra for a particular field within the EPR envelope of a frozen solution are associated with a well-defined subset of orientations, and simulations of a '2-D' set of such spectra can yield full hyperfine tensors (*33, 34*). Spectral simulations were done using the Bruker software WIN EPR.

## RESULTS

*EPR Signals Associated with Nitrogenase Reduction of $CS_2$.* Nitrogenase samples trapped by freezing after 90 s of turnover with $CS_2$ as the substrate showed new low-temperature X-band EPR inflections not associated with previously reported oxidation states of any of the metal clusters (Figure 1, trace 2). The inflection with $g_1 \sim 2.03$ was observed in our earlier studies at low protein concentrations (*21*). At the higher protein concentrations of the present study, two new EPR inflections were observed with $g_1 = 2.211$ and 2.111, as well as new features at $g = 1.996$, 1.973, and 1.956. A sample frozen under similar turnover conditions, but in the absence of $CS_2$ under an argon atmosphere (with protons as substrate), did not show any of these new signals. Instead it showed just the previously described weak intensity signals from the Fe protein $[4Fe\text{-}4S]^{1+}$ cluster and the resting state of FeMo cofactor (Figure 1, trace 1). The new signals observed for the trapped state during reduction of $CS_2$ absolutely required the presence of both nitrogenase component proteins, MgATP, and reductant. In addition, the product $H_2S$ did not induce any of these signals.

Combined analysis of the species trapped during reduction of $CS_2$ by use of Q-band (35 GHz) (Figure 2) and X-band (Figure 3) EPR spectroscopy allowed decomposition into three distinct subspectra, termed "a", "b", and "c". The Q-band spectrum shown in Figure 2 (panel A) is accompanied by a simulation generated by summing the three subspectra: "a" with $g$ values of [2.035, 1.982, 1.973]; "b"

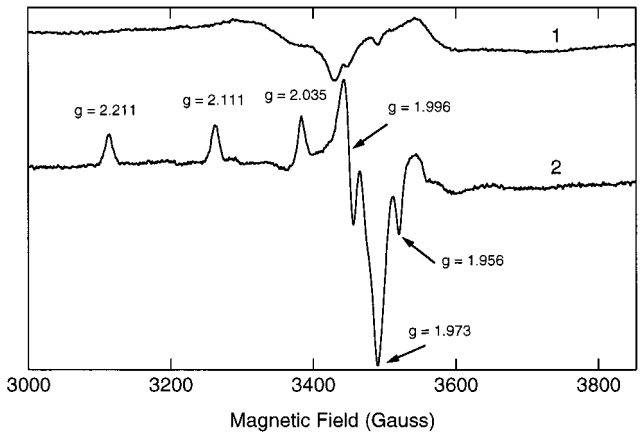


FIGURE 1: X-band EPR spectra of nitrogenase under turnover conditions. EPR spectra of nitrogenase under turnover conditions with protons (trace 1) or 1 mM $CS_2$ (trace 2) as substrate. Samples contained 250 $\mu$M MoFe protein in a complete reaction solution of 100 mM MOPS, pH 7.0, as described under Experimental Procedures. The reaction was initiated by the addition of Fe protein (125 $\mu$M) and allowed to proceed at 25 °C for 90 s before freezing in liquid nitrogen. The X-band EPR spectra were recorded at a temperature of 14 K, a microwave power of 250 $\mu$W, and a microwave frequency of 9.64 GHz, and represent the sum of 5 scans.

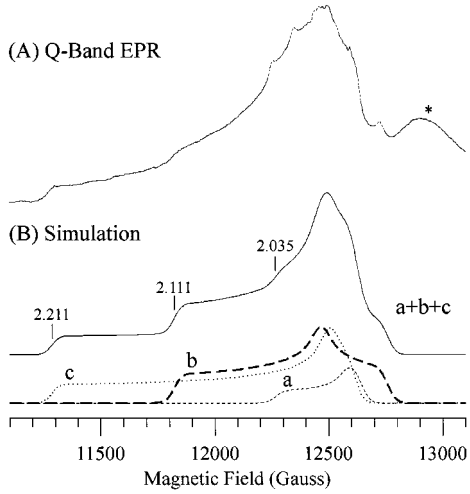


FIGURE 2: Q-band EPR spectrum and simulations of nitrogenase under turnover conditions with $CS_2$. Panel A: The Q-band EPR absorption spectrum for nitrogenase trapped 1 min after initiation of turnover with $CS_2$ is shown. The portion of the spectrum assigned to the Fe protein $[4Fe\text{-}4S]^{1+}$ cluster is noted with an "*". A small amount of contaminating Mn(II) is present in the sample and is indicated by the dashed line. The experimental conditions are microwave frequency = 34.998 GHz and modulation amplitude = 2.7 G and a temperature of 2 K. Panel B: Simulations for the components of the EPR spectrum shown in panel A are shown as dashed and dotted lines (a, b, c). The composite spectrum is shown as a solid line (a + b + c). The simulation parameters were the following: "a", $g$ = [2.035 1.982 1.973]; "b", $g$ = [2.111 2.002 1.956]; "c", $g$ = [2.211 1.996 1.978]; a line width of 20 G and an intensity ratio of "a":"b":"c" = 0.2:1.0:1.0.

with $g$ values of [2.111, 2.002, 1.956]; and "c" with $g$ values of [2.211, 1.996, 1.978]. The ratio of the simulated intensities for "a", "b", and "c" is 0.2:1:1. For the simulations, the additional contributions from the Fe protein $[4Fe\text{-}4S]^{+1}$ cluster and trace contaminating Mn were removed visually. Spectrometer settings were chosen to minimize contributions from the $S = 3/2$ state of FeMo cofactor.

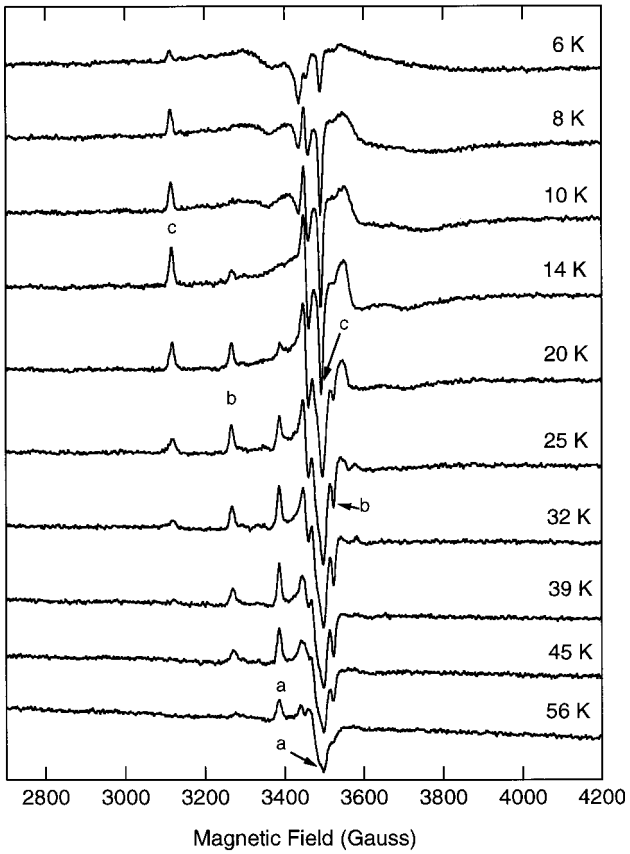


FIGURE 3: Temperature dependence, from 6 to 56 K, of the X-band EPR spectrum of nitrogenase under turnover conditions with $CS_2$. A nitrogenase sample during reduction of $CS_2$ was frozen 90 s after initiation of the reaction. X-band EPR spectra were recorded at a microwave power of 1 mW microwave, a microwave frequency of 9.64 GHz, and at the indicated temperatures. The sample contained 250 $\mu$M MoFe protein, 100 $\mu$M Fe protein, an initial $CS_2$ concentration of 1 mM, and a complete reaction mixture. Inflections associated with signals "a", "b", and "c" are noted.

The EPR signal intensities of "a", "b", and "c" depend strongly on the temperature of data collection, as illustrated in Figure 3, indicating that the distinct features of the species giving rise to the three signals extend to their relaxation properties. As a result, the temperature optimum for each signal is dependent on the microwave power, so the data in Figure 3 merely illustrate that the relation properties of each of the three $CS_2$-dependent species is different.

*Effect of Reaction Time on $CS_2$-Turnover EPR Signals.* Samples of nitrogenase were frozen at various times after initiation of the reduction of $CS_2$, and then X-band EPR spectra were collected at temperatures chosen to optimize the observation of each of the EPR active states: 10 K for "a", 25 K for "b", and 40 K for "c". Figure 4, which plots the relative signal intensity for each signal against the time of reaction, shows that the three EPR-active intermediates associated with $CS_2$ reduction appear and disappear sequentially following initiation of the reaction. Signal "a" appeared first, achieved maximal intensity at 25 s, and decreased in intensity after 60 s. Signal "b" increased and decreased between 50 and 100 s, whereas signal "c" reached maximal intensity after 100 s and decreased in intensity thereafter.

*Effects of Protein Component Ratio and $CS_2$ Concentration on EPR Signal Intensities.* The effects of changing the nitrogenase component protein ratio on the formation and

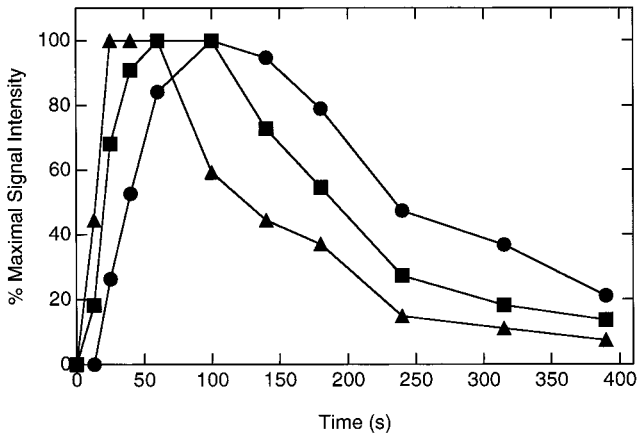


FIGURE 4: Time course for the appearance and disappearance of the three EPR signals attributed to $CS_2$ reduction. The relative intensities of the EPR signals "a" (▲), "b" (■), and "c" (●) are plotted against the time of reaction under $CS_2$. The signal intensity was quantified by measuring the peak-to-peak height for the $g = 2.03$ signal at 40 K, the $g = 2.11$ signal at 25 K, and the $g = 2.21$ signal at 10 K. Each peak height was normalized to the largest intensity value measured for the respective EPR inflection.

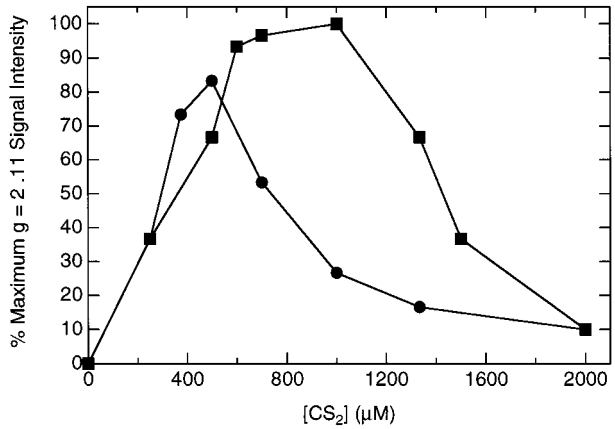


FIGURE 5: Effect of $CS_2$ concentration on the intensity of EPR signal "b". The effect of varying the $CS_2$ concentration, from 250 $\mu$M to 2 mM, on the normalized EPR intensity of signal "b" under nitrogenase reduction of $CS_2$ is presented with 100 $\mu$M MoFe protein and 50 $\mu$M Fe protein (●), or with 250 $\mu$M MoFe protein and 125 $\mu$M Fe protein (■). The intensities of the EPR signals were quantified by measuring the peak-to-peak height of the $g = 2.11$ inflection of signal "b", and normalized to the largest intensity value measured for the 250 $\mu$M MoFe protein containing samples. Assays were performed as described under Experimental Procedures except that the $CS_2$ concentrations were varied, as noted in the figure. Samples were frozen in liquid nitrogen at 60 s after the reaction was initiated. EPR spectra were recorded at a temperature of 12.5 K, a microwave power of 201 $\mu$W, and a microwave frequency of 9.64 GHz, and represent the sum of 5 scans.

intensities of the $CS_2$-dependent EPR signals were examined. Following the intensity of the "a" signal as representative of the new signals, it was observed that increasing the ratio of Fe protein to MoFe protein from 0.1:1 to 2:1 resulted in a near-hyperbolic increase in intensity, with maximal intensity observed for 1:1 and higher (not shown). Changes in the protein component ratio did not alter the relative intensities of "a" to "b" to "c" nor were changes in line shape ever observed.

The effect of initial $CS_2$ concentration on the intensity of the new EPR signals also was determined (Figure 5). For a molar ratio of Fe protein to MoFe protein of 0.5:1 at a MoFe protein concentration of 100 $\mu$M, a sharp maximum in the

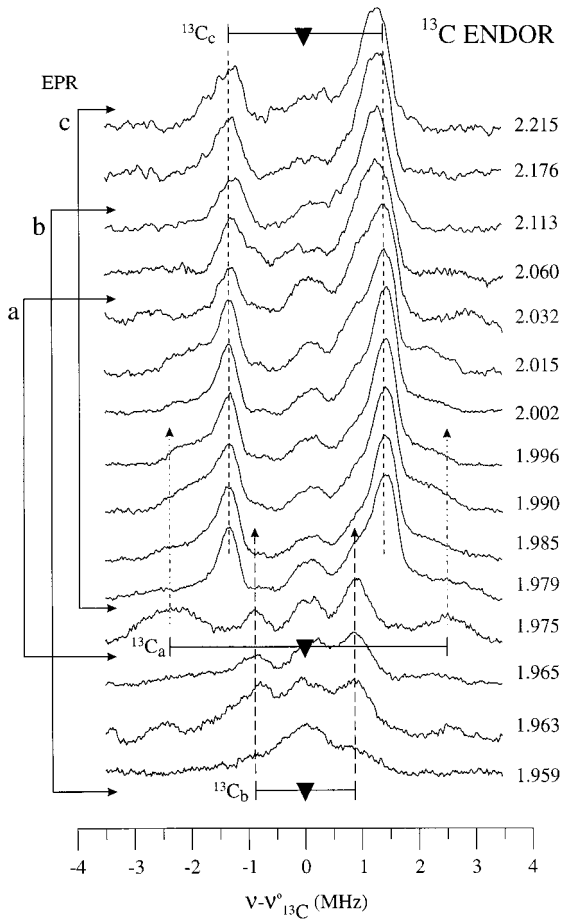


FIGURE 6: Q-band $^{13}C$ ENDOR spectra of nitrogenase under turnover conditions with $^{13}CS_2$. First-order ENDOR spectra are shown for corresponding $g$ values (right) and are centered at the $^{13}C$ Larmor frequency (▼). The brackets to the left indicate the corresponding EPR envelopes for spectra "a", "b", or "c". The three doublets (marked with "goal posts") have hyperfine coupling constants indicated by $^{13}C_a$, $^{13}C_b$, and $^{13}C_c$. Experimental conditions: microwave frequency, 34.933 GHz; modulation amplitude, 2.7 G; RF power, 20 W; RF sweep speed, 0.1 MHz/s; temperature, 2 K.

"a" signal intensity was observed when the initial concentration of $CS_2$ was ~500 $\mu$M. When the MoFe protein concentration was increased to 250 $\mu$M while maintaining a 0.5:1 molar ratio of Fe protein to MoFe protein, a broad maximum in the EPR intensity was observed near 1 mM $CS_2$.

*ENDOR of the $^{13}CS_2$ States.* To characterize the species formed under turnover with $CS_2$, CW Q-band $^{13}C$ ENDOR spectra were obtained across the EPR envelope of a sample that was quenched at 60 s after initiation of the reaction, and that contained high concentrations of all three species, "a", "b", and "c" (Figure 6). This set shows three distinct $^{13}C$ doublets (marked by "goal posts") centered at the $^{13}C$ Larmor frequency (▼) with hyperfine couplings of $A = 4.9$ MHz ($^{13}C_a$), 1.8 MHz ($^{13}C_b$), and 2.7 MHz ($^{13}C_c$). Although the individual EPR subspectra overlap strongly (Figure 2), at Q-band there is a low-field region that arises only from "c" and also a high-field region associated only with "b". As a result, it is possible to assign the three distinct $^{13}C$ doublets to the three EPR-active intermediates by following the appearance and disappearance of the ENDOR signals with field. Note that experiments with natural-abundance $CS_2$

show that the weak features at the $^{13}C$ Larmor frequency arise from naturally abundant matrix $^{13}C$.

The top two ENDOR spectra of Figure 6 are associated *only* with intermediate "c", as indicated. They show a doublet from a $^{13}C$ incorporated into this species, denoted $^{13}C_c$, whose hyperfine splitting of 2.7 MHz remains constant at fields throughout the EPR spectrum of "c", disappearing at higher fields. The three lowest spectra in Figure 6 are associated *only* with "b". They show a $^{13}C$ doublet from a fragment of $^{13}CS_2$, denoted $^{13}C_b$, with a hyperfine coupling constant of 1.8 MHz, as seen clearly at *g* values 1.975−1.963. This doublet also is seen as a shoulder on the inside of the $^{13}C_c$ doublet for the majority of fields where the EPR spectrum of "b" contributes, and thus is to be associated with a fragment of $^{13}CS_2$ bound to "b". Finally, as the field is lowered from the high-field edge of the composite EPR envelope, a broad $^{13}C$ doublet appears at the high-field edge of the "a" EPR component signal at g ∼ 1.975, which is thus assigned to a fragment of $^{13}CS_2$ incorporated into the intermediate that gives rise to EPR signal "a". This doublet has the largest hyperfine coupling seen in Figure 6: 4.9 MHz. As the field is lowered within the envelope of "a", this ENDOR signal becomes difficult to follow because of the appearance of the strong $^{13}C_c$ signal, although it clearly is present as a shoulder to the outside of that signal over most of the "a" EPR envelope. Overall, within the rather poor ability to follow the three $^{13}C$ signals across their respective EPR envelopes, the hyperfine couplings for the $^{13}C$ signals associated with each of the three intermediate species appear to be essentially isotropic.

## DISCUSSION

*Trapped Intermediates during $CS_2$ Reduction.* Nitrogenase reduces $CS_2$ to $H_2S$ and an unknown CS species at relatively low rates [157 nmol of substrate·min$^{-1}$·(mg of protein$^{-1}$)] when compared to $N_2$ or acetylene reduction rates [>2000 nmol of substrate·min$^{-1}$·(mg of protein$^{-1}$)]. However, $CS_2$ is an inhibitor of reduction of other substrates (e.g., protons), so electron flux through nitrogenase is directed to $CS_2$ reduction (*35*). Earlier, it was observed that if nitrogenase was rapidly frozen during reduction of $CS_2$, a new EPR-detectable species was observed with *g* values of 2.21, 1.99, and 1.97, denoted "c" here. This new signal was small compared to the signal arising from the resting state of FeMo cofactor at the protein concentration used in those experiments (11 mg of MoFe protein/mL). The present study shows that when the MoFe protein concentration is significantly increased (63 mg of MoFe protein/mL), additional EPR signals can be detected (Figure 1). High-field (Q-band) EPR allowed separation of these signals that were overlapping in the lower field (X-band) EPR spectrum. Simulations of the Q-band EPR spectrum (Figure 2) are best fit with three different EPR signals, which we have called "a", "b", and "c" (Table 1). As is summarized in Figure 4, a sequential increase and decrease in the intensity of each signal suggests the sequential appearance of the three species, implicating them as intermediates in the reduction of $CS_2$. It seems unlikely that the three species "a", "b", and "c" represent dead-end reaction intermediates as evidenced by the fact that each EPR spectrum declines in intensity over a fairly short time.

Table 1: Summary of Nitrogenase Turnover Intermediates Detected by EPR

| substrate/inhibitor[a] | | EPR signals (*g* values) | | | reference |
|---|---|---|---|---|---|
| $CS_2$ | a | 2.035 | 1.982 | 1.973 | this work |
| | b | 2.111 | 2.022 | 1.956 | this work |
| | c | 2.211 | 1.996 | 1.978 | this work |
| $H^+$ | V | 2.139 | 2.001 | 1.977 | (*15*, *16*) |
| | VII | 5.7 | 5.4 | | (*11*, *16*) |
| | VIII | 2.092 | 1.974 | 1.933 | (*16*) |
| $C_2H_2$ | Ic | 4.67 | 3.37 | 2.00 | (*16*) |
| $N_2$ | | 2.13 | 1.98 | | (*17*) |
| $C_2H_4$ | VI | 2.125 | 2.000 | 2.000 | (*16*, *42*) |
| CO | lo | 2.09 | 1.97 | 1.93 | (*15*, *17*−*20*) |
| | hi | 2.17 | 2.06 | 2.06 | |
| NO[b] | | 2.03 | 1.97 | 1.94 | (*43*) |

[a] The nomeclature used to identify each species is also presented. [b] NO reaction is with the MoFe protein alone in the absence of turnover.

The relatively low optimum temperature for the observation of each signal (<50 K) is most consistent with each arising from a metal cluster. The fact that the *g* values observed for the $CS_2$ sample do not correspond to any of the *g* values previously assigned to metal clusters of nitrogenase or that have been observed during turnover with other substrates or inhibitors (Table 1) suggests that the new signals arise from unique intermediates with $CS_2$, or a reductive product, bound to one of the nitrogenase metal clusters. However, the lack of appearance of any of the three new $CS_2$-dependent EPR signals upon addition of $H_2S$, and the $^{13}C$-ENDOR effect rule out $H_2S$ binding accounting for any of the EPR signals.

To characterize these intermediates, we employed $^{13}CS_2$ as the substrate and used $^{13}C$ ($I = 1/2$) ENDOR spectroscopy to determine if a $^{13}C$-bearing species is associated with the intermediates. Figure 6 shows that each of the three EPR signals gives a single $^{13}C$-ENDOR doublet centered at the Larmor frequency for $^{13}C$. Furthermore, each of the doublets had a unique hyperfine coupling constant. These results are most consistent with the three intermediates shown by EPR spectroscopy to occur during $CS_2$ reduction containing a metal-bound carbon-bearing fragment. The magnitudes of the hyperfine couplings observed here are comparable to the $^{13}C$ hyperfine couplings (1−5 MHz) observed from $^{13}CO$ binding to FeMo cofactor (*19*, *20*) while the hyperfine coupling constants observed for $^{13}CO$ or $^{13}CN$ bound to the active sites of other metalloenzymes (e.g., hydrogenase or CO dehydrogenase) typically are significantly larger (>20 MHz). This, in the context of the fact that the active site for $N_2$ reduction is on the FeMo cofactor, leads us to suggest that the three EPR-active, carbon-bound intermediates observed for $CS_2$ reduction are associated with the FeMo cofactor.

*Nitrogenase Mechanism of Substrate Reduction.* The present work is most consistent with the sequential appearance of three distinct states of the FeMo cofactor with a carbon-bound species during the reduction of $CS_2$ by nitrogenase. Theoretical calculations and comparisons to model compounds have been used to suggest several different models for how substrates bind to and are reduced at FeMo cofactor of nitrogenase (*36*−*38*). Two competing models hold that substrates bind either to the Mo after a ligand is released or to one or more of the three coordinate Fe atoms around the "waist" of FeMo cofactor. The $^{13}CO$ ENDOR study of intermediate states formed under turnover conditions

in the presence of the inhibitor CO (*19*, *20*) was interpreted as indicating that CO binds to Fe atoms of the FeMo cofactor in two alternate modes: one CO binds as a bridging ligand to waist Fe atoms in the so-called 'lo-CO' intermediate, while two bind as terminal ligands in the 'hi-CO' intermediate.

Extensive work has been done with $CS_2$ as ligands to various model compounds that may provide some insights into the types of intermediates that might be generated during nitrogenase reduction of $CS_2$ (*39*). In most of these model compounds, bonding is observed to be through the carbon, as, for example, in **1** (*40*). Likewise, $CS_2$ can bridge between

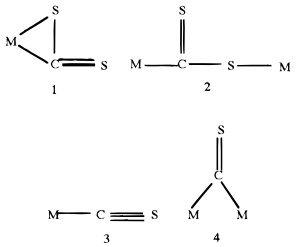

two or more metals, as in **2**. Such bonding intermediates could be easily envisioned for $CS_2$ binding to FeMo cofactor (e.g., to two Fe atoms at the waist). In either case, the binding to Fe through the carbon would account for the $^{13}$C-ENDOR effect observed here for the three intermediates. Given that $H_2S$ is one of the products of $CS_2$ reduction by nitrogenase, it is reasonable to predict a thiocarbonyl intermediate bound to the active site (such as **3** or **4**). Given that thiocarbonyl is similar in many ways to CO (*41*), it is reasonable to propose that a CS intermediate bound to FeMo cofactor would be similar to that proposed for CO binding (*19*). However, in our study of CO-bound intermediates, we suggested that nearly isotropic $^{13}$C tensors would be more likely to arise with $^{13}$CO, and hence $^{13}$CS, bound as terminal, rather than bridging ligands (*20*). Thus, it would be plausible to suggest that the first intermediate formed, "a", contains a species such as **1**, while the last intermediate, "c", is more likely to contain **3**. The species **4** seems unlikely to correspond to the intermediates we observe, whereas **2**, by virtue of its binding of C to a single Fe, probably cannot be discounted.

## ACKNOWLEDGMENT

We thank Dr. William N. Lanzilotta and Ms. Jeannine M. Chan for assistance in purifying proteins used in this study and Drs. Jennifer E. Huyett and Jason Christiansen for helpful discussions.

## REFERENCES

1. Ferguson, S. J. (1988) in *The Nitrogen and Sulphur Cycles* (Cole, J. A., and Ferguson, S. J., Eds.) pp 1−30, Cambridge University Press, Cambridge, U.K.
2. Hadfield, K. L., and Bulen, W. A. (1969) *Biochemistry 8*, 5103−5108.
3. Rivera-Ortiz, J. M., and Burris, R. H. (1975) *J. Bacteriol. 123*, 537−545.
4. Simpson, F. B., and Burris, R. H. (1984) *Science 224*, 1095−1097.
5. Thorneley, R. N. F., and Lowe, D. J. (1985) in *Molybdenum Enzymes* (Spiro, T. G., Ed.) pp 221−284, Wiley, New York.
6. Kim, J., and Rees, D. C. (1992) *Nature 360*, 553−560.
7. Shah, V. K., and Brill, W. J. (1977) *Proc. Natl. Acad. Sci. U.S.A. 74*, 3249−3253.
8. Chan, J. M., Christiansen, J., Dean, D. R., and Seefeldt, L. C. (1999) *Biochemistry 38*, 5779−5785.
9. Peters, J. W., Fisher, K., Newton, W. E., and Dean, D. R. (1995) *J. Biol. Chem. 270*, 27007−27013.
10. Lanzilotta, W. N., and Seefeldt, L. C. (1996) *Biochemistry 35*, 16770−16776.
11. Lowe, D. J., Fisher, K., and Thorneley, R. N. F. (1993) *Biochem. J. 292*, 93−98.
12. Ma, L., Brosius, M. A., and Burgess, B. K. (1996) *J. Biol. Chem. 271*, 10528−10532.
13. Georgiadis, M. M., Komiya, H., Chakrabarti, P., Woo, D., Kornuc, J. J., and Rees, D. C. (1992) *Science 257*, 1653−1659.
14. Thorneley, R. N. F., Eady, R. R., and Lowe, D. J. (1978) *Nature 272*, 557−558.
15. Yates, M. G., and Lowe, D. J. (1976) *FEBS Lett. 72*, 121−126.
16. Lowe, D. J., Eady, R. R., and Thorneley, R. N. F. (1978) *Biochem. J. 173*, 277−290.
17. Davis, L. C., Henzl, M. T., Burris, R. H., and Orme-Johnson, W. H. (1979) *Biochemistry 18*, 4860−4869.
18. Pollock, C. R., Lee, H.-I., Cameron, L. M., DeRose, V. J., Hales, B. J., Orme-Johnson, W. H., and Hoffman, B. M. (1995) *J. Am. Chem. Soc. 117*, 8686−8687.
19. Christie, P. D., Lee, H. I., Cameron, L. M., Hales, B. J., Orme-Johnson, W. H., and Hoffman, B. M. (1996) *J. Am. Chem. Soc. 118*, 8707−8709.
20. Lee, H. I., Cameron, L. M., Hales, B. J., and Hoffman, B. M. (1997) *J. Am. Chem. Soc. 119*, 10121−10126.
21. Rasche, M. E., and Seefeldt, L. C. (1997) *Biochemistry 36*, 8574−8585.
22. Seefeldt, L. C., Morgan, T. V., Dean, D. R., and Mortenson, L. E. (1992) *J. Biol. Chem. 267*, 6680−6688.
23. Burgess, B. K., Jacobs, D. B., and Stiefel, E. I. (1980) *Biochim. Biophys. Acta 614*, 196−209.
24. Seefeldt, L. C., and Mortenson, L. E. (1993) *Protein Sci. 2*, 93−102.
25. Hathaway, G. M., Lundak, T. S., Tahara, S. M., and Traugh, J. A. (1979) *Methods Enzymol. 60*, 495−511.
26. Chromy, V., Fischer, J., and Kulhanek, V. (1974) *Clin. Chem. 20*, 1362−1363.
27. Seefeldt, L. C., and Ensign, S. A. (1994) *Anal. Biochem. 221*, 379−386.
28. Werst, M. M., Davoust, C. E., and Hoffman, B. M. (1991) *J. Am. Chem. Soc. 113*, 1533−1538.
29. Feher, G. (1959) *Phys. Rev. 114*, 1219−1244.
30. Mailer, C., and Taylor, C. P. S. (1973) *Biochim. Biophys. Acta 322*, 195−203.
31. Hoffman, B. M., DeRose, V. J., Ong, J.-L., and Davoust, C. E. (1994) *J. Magn. Reson. Ser. A 110*, 52−57.
32. Abragam, A., and Bleany, B. (1970) *Electron Paramagnetic Resonance of Transition Ions*, 2nd ed., Clarendon Press, Oxford, U.K.
33. Hoffman, B. M., DeRose, V. J., Doan, P. E., Gurbiel, R. J., Houseman, A. L. P., and Telser, J. (1993) *Biol. Magn. Reson. 13*, 151−218.
34. DeRose, V. J., and Hoffman, B. M. (1995) *Methods Enzymol. 23*, 555−589.
35. Seefeldt, L. C., Rasche, M. E., and Ensign, S. A. (1995) *Biochemistry 34*, 5382−5389.
36. Dance, I. G. (1994) *Aust. J. Chem. 47*, 979−990.
37. Sellmann, D., and Sutter, J. (1996) *J. Biol. Inorg. Chem. 1*, 587−593.
38. Coucouvanis, D. (1996) *J. Biol. Inorg. Chem. 1*, 594−600.
39. Cotton, F. A., Wilkinson, G., Murillo, C. A., and Bochmann, M. (1999) *Advanced Inorganic Chemistry*, 6th ed., John Wiley and Sons, New York.
40. Pandey, K. K. (1995) *Coord. Chem. Rev. 140*, 37−114.
41. Moltzen, E. K., and Klabunde, K. J. (1988) *Chem. Rev. 88*, 391−406.
42. Hawkes, T. R., Lowe, D. J., and Smith, B. E. (1983) *Biochem. J. 211*, 495−497.
43. Hyman, M. R., Seefeldt, L. C., Morgan, T. V., Arp, D. J., and Mortenson, L. E. (1992) *Biochemistry 31*, 2947−2955.

BI9919100